IL NUOVO CIMENTO **48 C** (2025) 48

Experimental search for high-spin resonant states in collisions of $^{28}\mathrm{Si} + {}^{12}\mathrm{C}$ at 35 MeV/nucleon, using FAUST array

R. Wada(*)

Cyclotron Institute, Texas A&M University - College Station, TX 77843, USA

received 26 November 2024

Summary. — A search for high-spin resonant states in highly excited ^{28}Si is performed, using an inverse reaction of $^{28}\mathrm{Si} + {}^{12}\mathrm{C}$ at 35 MeV/nucleon. Twelve possible candidate peaks in different seven-α decay channels, particularly those involving ^{8}Be(gs and 2+) emission are suggested as such resonances in the sub μb range of cross-section. Utilizing a shape analysis method, a χ^2 fit is performed comparing the experimental events in each resonant peak to those of simulated events with particular shapes and angular momenta. The shapes and angular momenta of the simulated event set at the χ^2 minimum are taken as those of the candidate peaks. For nine of the candidate peaks their optimum shapes and angular momenta are suggested. The trend of the evaluated excitation energy *vs.* angular momentum agrees well with that of the theoretical toroidal high-spin states predicted by Ren *et al.*, *Nucl. Phys. A*, **996** (2020) 121696, but the minimum χ^2 fits to the experimental data suggest tube shapes not toroids as the optimal disassembling shapes.

1. – Introduction

Toroidal high-spin isomer states as an extreme case of nuclear deformation have been studied theoretically in pioneering works of Wong [1-3] in a wide range of nuclei. In the 1970 s and in his recent work with Staszczak, stabilized toroidal isomer states are predicted within a mean-field calculation [4] for $N = Z$ nuclei in a mass range of $28 \leq A \leq 52$. A study, made recently by Ren *et al.* [5], using a mean-field–based covariant density functional theory calculation in three-dimensional lattice space results in similar predictions.

Experimentally in our previous work in ref. [6], the possible existence of three high-spin isomers with estimated cross-sections of 30–50 μb was reported in the seven-α decay channel of the highly excited ^{28}Si projectile in an inverse kinematic reaction of $^{28}\mathrm{Si} + {}^{12}\mathrm{C}$ at 35 MeV/nucleon. The observed resonant energies agree well with those predicted in ref. [4] for toroidal shapes. However no further experimental characterization of these

(*) E-mail: wada@comp.tamu.edu

resonances was possible, especially for their physical shape and angular momentum, just because of low statistics.

To verify the above experimental results with higher position resolution and better statistics, the same reaction was studied with the upgraded FAUST array. A recent paper, ref. [7], based on that experiment, concluded that no strong evidence was observed for such resonances above the $20\,\mu$b range and characterized smaller peaks as statistical fluctuations. However, such conclusions are strongly dependent on assumptions regarding background subtractions. In the sub μb range, strong correlations are, in fact, observed among peaks in the excitation energy distributions of the subsets of seven-α events exhibiting signals of ^{8}Be(gs and 2+) precursors during disassembly. These peaks are identified as the candidate peaks for high-spin resonant states, and in this contribution I will present recent results for characterization of their physical shapes and angular momenta.

2. – Experiment

The same reaction as ref. [6], ^{28}Si+^{12}C at 35 MeV/nucleon, was studied with much higher statistics and higher position resolution in the excitation energy reconstruction, utilizing the newly upgraded FAUST (Forward Array using Si Technique) array [7]. The array consists of 68 Si-CsI telescopes in five concentric square rings [8]. This original array has been upgraded in two ways. The newly upgraded array is equipped with a position sensitive Si detector (dual-axis dual lateral) for all telescopes, to determine the X-Y position of particle within the 2 cm $\times$ 2 cm Si detector with a position resolution of 0.4 mm for alpha particles in each direction [7, 9, 10]. This results in the fact that, since the energy resolution of each alpha particle is of an order of 100 keV, the energy resolution in the excitation energy reconstruction from seven-α particles is proportional to its absolute value, and changes from 1 to 2.5 MeV when the reconstructed excitation energy changes from 60 to 160 MeV, respectively [7]. Another upgrade is made for the data acquisition system. Using Struck VME fast sampling digitizer SIS3316, multi-event trigger is accomplished, which realizes almost no dead time for the data acquisition and more than 10k counts/sec operation [10]. In the actual experiment, however, about 2k counts/sec data taking rate was maintained to minimize radiation damage in the most forward Si array. With this data rate, more than 340M events with particle identification and position determination were recorded. The excellent position resolution enables identification of ^{8}Be(gs and 2+) in the relative velocity spectrum of any two α pairs. These identified α pairs are utilized to further classify the seven-α events into subset groups in this work.

3. – Shape analysis in momentum space

For the shape characterization of the experimental data, shape analysis in momentum space is utilized. The shape analysis is based on the extraction of eigenvalues $\lambda_1, \lambda_2, \lambda_3$ of the 3×3 tensor $T_{ij} = \Sigma(C_i^m C_j^m)$, where C_i^m is either coordinate or momentum vector of each constituent particle, $i, j = (x, y, z)$ and m is the particle multiplicity in a given event. These eigenvalues characterize the shape of each event. Using these eigenvalues, sphericity S and coplanarity C are defined as a linear combination of them so that a perfect sphere, rod and disk correspond to the three corners of a triangle $(S, C) = (1, 0), (0, 0), (3/4, \sqrt{3}/4)$, respectively, when C_i^m are taken

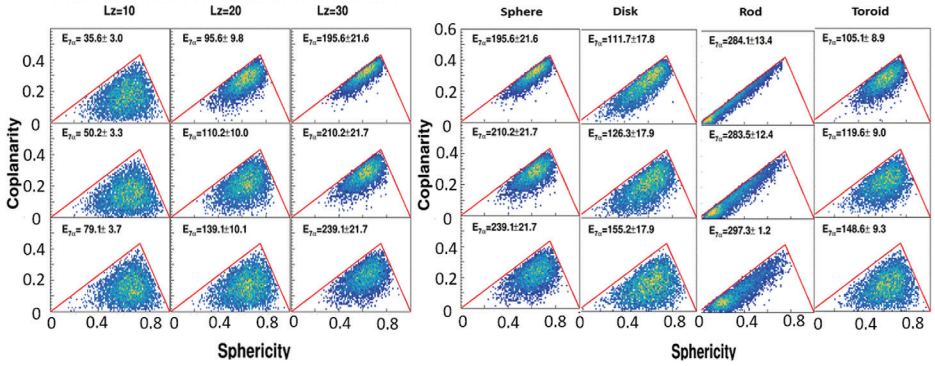

Fig. 1. – (Color online). Left: momentum shape distributions in sphericity-coplanarity plots for events from a spherical seven-α nuclei, corresponding to $E_{th} = 0.5, 1.0, 2.0\,\mathrm{MeV/nucleon}$ from top to bottom row and $L_z = 10, 20, 30\hbar$ from left to right. Total kinetic energy is also shown in each figure. Right: momentum shape distributions in sphericity-coplanarity plots for events with sphere, disk, rod, toroid from left to right with $L_z = 30\hbar$. Total kinetic energy is also shown in each figure.

from the coordinate vectors. However when C_i^m are taken from the momentum vector, direct correlation between the location (S, C) and their physical shape is lost in general.

Momentum shape distributions for a spherical shape are plotted in fig. 1 (left) for the thermal energy E_{th}, which is a part of the available excitation energy and the rest becomes the rotational energy, $E_{th} \sim 0.5, 1.0, 2.0\,\mathrm{MeV/nucleon}$ from top to bottom row and $L_z = 10, 20, 30\hbar$ from left to right column. The event sets are generated in a similar way as those described in sect. **5** for a given spherical shape. The general trend discussed here is common to all shapes dealt later. For $L_z = 10\hbar$ on the left panel, (S, C) values show a broad distribution around the center and are similar for different E_{th}. This is because the momentum distribution is governed by the random thermal motion and the momentum is normalized in the shape analysis. When L_z values increase, the distribution shifts toward the rod-disk line (left-upper side of the triangle). This observation indicates that the distance from the (S, C) point to the rod-disk line, referred as Δ_{RD} hereafter, relates inversely to the angular momentum and can be used to enhance the events with possible high-spin state resonances.

4. – Experimental results

4˙1. *Origin and cross-sections of seven-α events.* – In fig. 2(a), the experimental α multiplicity distributions are compared with the results of unfiltered and filtered AMD [11-13] calculations on an absolute scale (mb). The absolute cross-sections for the experimental results are obtained, assuming the total number of the experimental events recorded corresponds to that of the AMD simulation of the impact parameter range of $0-7\,\mathrm{fm}$, which gives a total cross-section of $1538\,\mathrm{mb}$. The experimental cross-section of the seven-α events (red-dashed histogram) is about $1\,\mathrm{mb}$, which is about a factor of 3 smaller than that of the AMD filtered cross-section (black histogram).

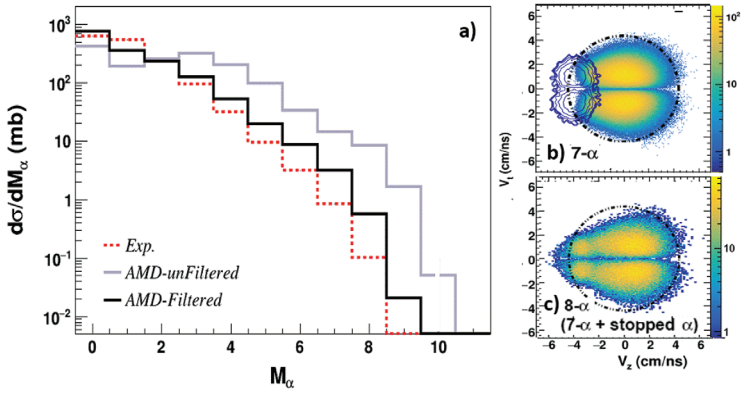

Fig. 2. – (Color online). (a) α multiplicity distributions are presented in an absolute scale from the experiment (red-dashed histogram), the non-filtered AMD (gray) and the AMD filtered through the experimental filter (black). (b) α velocity distribution V_z *vs.* V_t for the seven-α events. The contours are those from the stopped α in Si. (c) Similar plot as (b), but for eight-α events with the stopped α. For the dot-dashed circles see the text.

In fig. 2(b) and (c), 2D plots of α velocity distributions for seven- and eight-α events are presented in their respective rest frame. The horizontal axis is the beam direction. In the latter α particles stopped in the front Si detector are included. The α particles from the target are clearly separated in (c), indicating that the majority of the seven-α events in (b) originate from the break up of the ^{28}Si projectile. The dot-dashed circles in (b) and (c) show the velocity cut made to exclude pre-equilibrium α particles as well as those from the target-like source in ref. [6]. The stopped α particles are not included in the following study of the seven-α events.

4˙2. *Candidate resonant peaks.* – Statistical analyses similar to that in ref. [7] are performed for six subsets of seven-α events and presented in fig. 3. In the top 6 panels, the standard deviations (SD) of the excitation energy distribution after subtracting the averaged distribution are shown for different decay paths. The averaged distribution for each set is obtained with polynomial fits used in ref. [7]. In order to enhance the events with possible high angular momentum states, the tighter condition $\Delta_{RD} \leq 1.0$ is applied for all except for (d), since in (d) the number of the events is small. Note that these event sets are exclusive from each other, that is, no event overlaps in these event sets. In the individual energy channel standard deviations, $\sigma_{SD} \geq 1.0$ can be used as a criterion of significant deviation. This is reasonable if the spectrum were to have a non-fluctuating background. With the statistical fluctuations, however, the deviations occur in both the positive and negative direction from the average and modify the "background" for resonant peaks. Therefore in this work the relative $\sigma_{SD} \geq 1.5$ measured from the nearest valley on either side of the peak is used as a criterion in addition to the same peak energy within 1 MeV. The observed peaks are fit by a Gaussian with its width $\sigma_G = 1.25 \pm 0.25$ (FWHM 2.97 ± 0.59 MeV) to guide the eye and shown by red curves in the figure. Adopting a relative standard deviation sigma $\sigma_{SD} \geq 1.5$, more than three cross correlations are required for the candidate resonant peaks, since three cross correlations are less probable in the statistical fluctuations alone. At this point twelve "candidate" peaks are identified as shown by the shaded blue and green bars

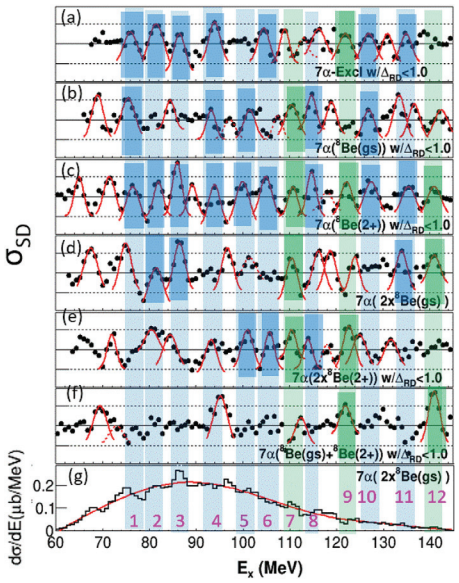

Fig. 3. – (Color online). Candidate resonant peaks identification. On the top 6 panels the standard deviations of the excitation energy distribution after subtracting the averaged distribution are shown for (a) exclusive seven-α events, where events decaying through any cluster formation are excluded, those decaying through (b) a single ^{8}Be(gs), (c) a single ^{8}Be(2+), (d) two-^{8}Be(gs), (e) two-^{8}Be(2+), (f) one ^{8}Be(gs) plus one ^{8}Be(2+). In all of them except for (d) the condition of $\Delta_{RD} \leq 1.0$ is applied. See more details in the text.

and observed cross correlation peak locations are indicated by darker short color bars. Those with blue bars are identified in this work and those with green bars, identified in our previous work in ref. [6], are also confirmed in this work. In the bottom panel, the excitation energy distribution for the events decaying through two ^{8}Be(gs) is shown for a comparison with the averaged distribution calculated from the polynomial fit. Identified peaks are numbered for convenience and indicated in the figure. The average probability for observing the corresponding candidate peak in each shaded long bar is about 50%. This indicates that the cross correlations are detectable among only some of the data sets. This reflects the fact that the resonant peaks are subject to the statistical fluctuations in general, making it problematic to identify the high-spin state resonances from the peak structure alone. Therefore in a further analysis I proceed by initially retaining these peaks as "candidate" high-spin state resonances, each of which corresponds to a specific physical shape and angular momentum, and carry this information over to an analysis of the observed seven-α particle energy spectra. In the following section the procedures to further characterize the shapes and angular momenta of these candidate peaks are described.

5. – Simulated event sets

Utilizing a shape analysis method [14], simulated event sets are generated in two steps to characterize these candidate resonant peaks, focusing on their physical shapes and angular momenta. In the first step, different shapes of nuclei initially corresponding

to seven-α particles are generated using the Extended Quantum Molecular Dynamics (EQMD) code of Maruyama *et al.* [15]. EQMD uses a Pauli potential to respect the Pauli principle and can generate the lowest energy state for initial nuclei. The initial nuclei are generated from randomly distributed nucleons in a sphere by a frictional cooling method. For the ^{28}Si case, 80% of the nuclei end up to a seven-α configuration within the cooling time of 2000 fm/c and 98% within 100000 fm/c. Fluctuations in their cooling process generate different shapes. In order to determine their physical shapes, a shape analysis method in coordinate space is utilized. About 80% of the generated initial nuclei have a disk shape. 15% are categorized as spherical. 1% are in a rod shape. The remaining 4% are distributed around the center in the sphericity-coplanarity plot with no distinct shapes and excluded for the analysis below. The nuclei with toroidal shapes are made from the disk-shaped nucleus by excluding nuclei which have α (or α particles) within a radius of 1.5 fm from the Z-axis. Similarly, tube-shaped nuclei (non-linear chains) are made from the rod-shape nuclei by excluding those with α particle(s) within a distance 1.0 fm from the Z-axis. Less than a few % remain in the latter two treatments. For each category, more than 5 k initial nuclei are generated. All shapes are made symmetric around the Z-axis.

The second step is to give kinetic energy to α particles in a given initial nucleus at a given excitation energy. Note that the seven α particles in the initial nuclei generated by EQMD do not initially have kinetic energy. For a candidate resonant peak at the excitation energy E_x, the available energy for the kinetic energy is given by $E_{av} = E_x - Q$. Q is the reaction Q value of ^{28}Si decaying into seven-α particles. E_{av} is divided into two parts, thermal kinetic energy and rotational energy.

1) The thermal energy E_{th} is set from 1 MeV to E_{av} in every 1 MeV step for simulated event sets at a given excitation energy and a shape. For each E_{th}, the rotational energy E_{rot} is given uniquely by $E_{rot} = E_{av} - E_{th}$. In order to make a clear separation between the thermal and rotational energies, the total angular momentum L is required, $|L| < 2$ to $5\hbar$ from $|L| \leq 20$ to $|L| = 50\hbar$ at the end of this procedure.

2) The rotational energy is given by rotating the whole seven-α system around the Z-axis, adjusting L_z to get E_{rot}. For a given E_{rot}, L_z value becomes different for different shapes, since their moments of inertia are different.

6. – Different shapes in momentum shape analysis

To evaluate the physical shapes of seven-α events in the experimental data set, the momentum shape distributions and those of the coordinate shapes are further explored, using the event sets generated in the previous sect. **5** for different shapes. In fig. 1 (right), the momentum shape distributions for different shapes are plotted with a given $L_z = 30\hbar$. When the thermal energy is low as shown on the top row, all distributions tends not only to distribute close to the rod-disk line (left-upper side of the triangle), following the general trend discussed in sect. **3**, but also to distribute differently along the line, especially for rods. This observation provides the distance from the (S, C) point to the disk-sphere line (right-upper side), referred to as Δ_{DS} hereafter, as a possible observable to distinguish different physical shapes, especially those between rods and others. When the thermal energy increases up to 2 MeV/nucleon, all distributions are shifted toward the center to a different extent. For rods, which have the least moment of inertia, the least shift is observed. For others, the whole distributions become more

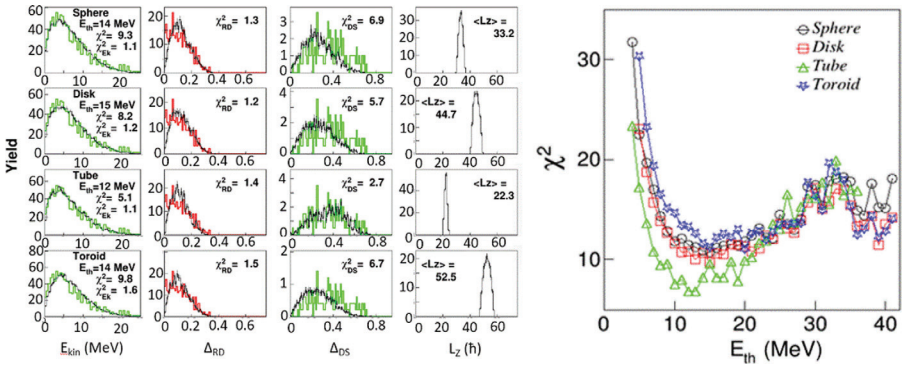

Fig. 4. – (Color online). An example of the χ^2 fit for the candidate resonant peak at $E_x = 86.5\,\mathrm{MeV}$. Left: colored histograms are from the experiment and black ones from the simulation. χ^2 in the left figure is given by $\chi^2 = \chi^2_{EK} + \chi^2_{\Delta_{RD}} + \chi^2_{\Delta_{DS}}$. Each χ^2 value is also given in each figure. $\langle Lz \rangle$ is the extracted average angular momentum. Right: χ^2 value distribution as a function of E_{th} for different shapes.

or less like each other, indicating that the thermal motion governs the distributions even for $L_z \leq 30\hbar$.

7. – Evaluation of shape and angular momentum

Each set of the simulated events in sect. **4** is compared to the events in the candidate peak to determine their shape and L_z one by one. Three observables are used for this purpose, α kinetic energy E_α in the seven-α rest frame, distance Δ_{RD} from the rod-disk line and distance Δ_{DS} from the disk-sphere line in the sphericity-coplanarity plot from the momentum shape analysis. The shape and L_z value of the simulated data set at the minimum χ^2 fit are taken to be those of each candidate resonant peak. In this talk, seven-α events with 2-^{8}Be(gs) decay path shown in the bottom of fig. 3 are used for the evaluation of the shapes and momenta of the candidate peaks.

In fig. 4 an example of the χ^2 fit is shown for the candidate resonant peak at $E_x = 86.5\,\mathrm{MeV}$ for the above seven-α events with a condition of $\Delta_{RD} \leq 0.10$. On the left, the experimental results from the events associated with the candidate resonant peak (colored histograms) and the fit results from the simulated events (black histograms) at

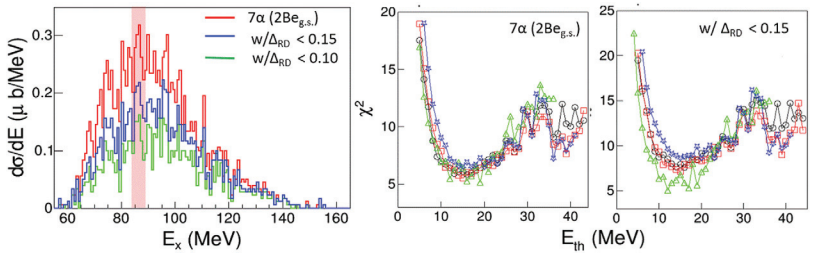

Fig. 5. – (Color online). Left: excitation energy distribution for seven-α events decaying through two-^{8}Be (red) and those with a condition $\Delta_{RD} \leq 0.15$ (blue) and $\Delta_{RD} \leq 0.10$ (green). Middle: χ^2 value distribution for the blue data set. Right: that for the green data set.

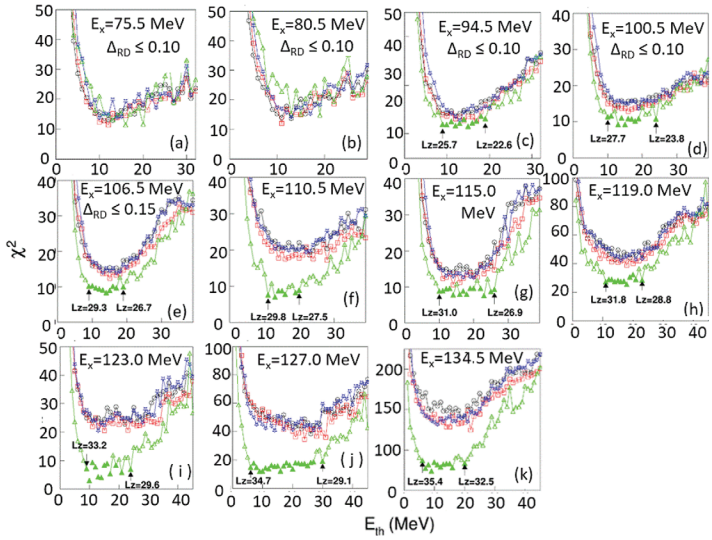

Fig. 6. – (Color online). Summary of χ^2 fit for the candidate resonant peaks, except that shown in fig. 4. L_Z values are evaluated from the bottom flat region with $\chi^2 \leq 1.3 * \chi^2_{min}$, which are indicated by solid green triangles and L_Z values at both ends are given in each figure.

the minimum χ^2 value are shown. The colored experimental data in each row are the same from the top to the bottom. In this example a tube shape is used instead of a rod, which results in a smaller χ^2 value in all cases. A further comparison between tube and rod will be made in sect. **8**. On the right, χ^2 values are plotted as a function of E_{th}. The preference of the tube shape is observed as shown. Note that this preference mainly originates from the better reproduction of Δ_{DS} on the third column in the left panel, where the center of the broad peak is properly reproduced, but other shapes do not.

A further study for the above preference is made for the same resonant peak under different conditions. Plotted on the left side of fig. 5 is the experimental excitation energy distributions of seven-α events with 2-^{8}Be(gs) with no condition (red histogram), with a looser condition of $\Delta_{RD} \leq 0.15$ (blue) and a slightly tighter one of $\Delta_{RD} \leq 0.10$ (green) on the distance Δ_{RD}. In fig. 5 the results of the green histogram (tighter condition) are presented. On the middle and right of fig. 5, similar plots to the right panel of fig. 4 are made for the red (no condition) and blue (looser condition) spectra from the middle to the right, respectively. For the experimental events from the red spectrum on the left, no shape preference is observed, whereas for those from the blue spectrum with the looser condition, a tube-shape preference similar to that with the tighter condition in fig. 4 is observed. These observations can be explained as follows. For no condition (the red spectrum), a dominant contribution from the non-resonance events is made to the shape distribution. When the looser condition $\Delta_{RD} \leq 0.15$ is applied, the non-resonant contribution becomes less, but that of the associated resonance remains more or less the same, as seen in its spectrum. When the tighter condition is applied, a larger fraction of the selected events results from the resonance and more enhancement of the preference than that shown on the right of fig. 4. This observation indicates that the events associated with the candidate resonant peak consist of both resonant and non-resonant components and the resonant component has a shape preference, but non-resonant events do not since they have essentially random nature. This is a strong

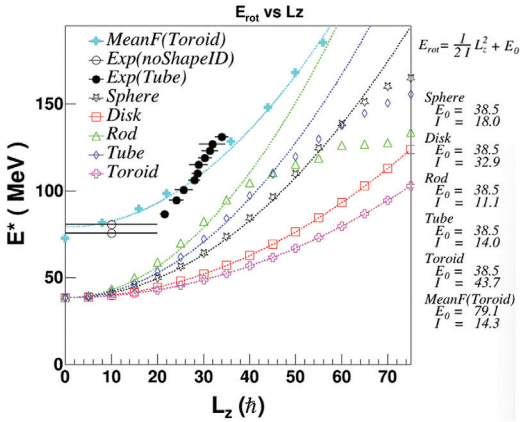

Fig. 7. – (Color online). Summary plot for the excitation energy and extracted L_z value of the candidate resonant peaks (open and closed circles) together with the theoretical predictions of Ren *et al.* [5] (light blue cross). Rotational energies for each shape of seven-α events. Parameters are listed on the right.

evidence that the candidate resonant peak originates from a high-spin resonant state on the top of the non-resonant component.

The minimum χ^2 search is made for all other candidate peaks. The results are summarized in fig. 6. These observations lead to the following remarks.

1) The two candidate peaks at $E_x \leq 80.5\,\mathrm{MeV}$ are low-spin states with angular momentum with $L_z < 20\hbar$. In such cases, no shape preference can be determined from the momentum shape analysis, since the momentum is dominated by the random thermal motion and the results from different physical shapes become similar to each other.

2) Three of those at $86.5 \leq E_x \leq 106.5\,\mathrm{MeV}$ consist of two distinct contributions, one from a resonance with a given physical shape and a high angular momentum, and the other from non-resonant component with random nature. Under the condition on Δ_{RD}, the former contribution becomes manifested in the χ^2 fit and the tube-shape preference is obtained.

3) Six of those at $E_x \geq 110.5\,\mathrm{MeV}$, except the one at 140 MeV, are dominated or have large enough contribution from a resonance component so that the χ^2 fit reveals the significant tube shape preference without any additional conditions. For that at 140 MeV, no analysis is made because of poor statistics.

The shapes and angular momenta of the simulated events at the minimum χ^2 fit are given as those of each candidate resonant peak and summalized in fig. 7. The extracted L_z values show a good agreement with those of the theoretically predicted by Ren *et al.* in their mean field calculation [5], although their calculations are made for toroidal shapes, not for tube shapes.

8. – Discussions: rod or tube shapes

In the previous section, tube shapes are used to get the minimum χ^2 search, instead of rod shapes. In fig. 8, the results of rod and tube shapes are presented for the candidate

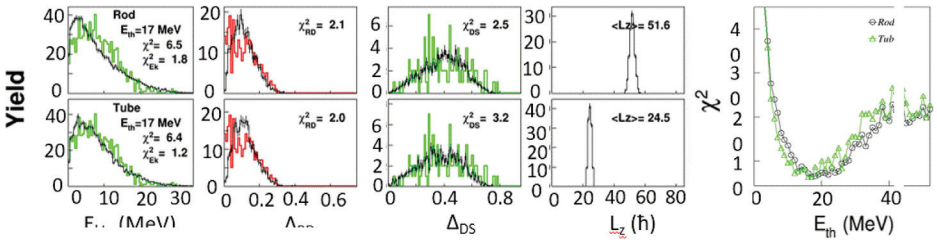

Fig. 8. – (Color online). Left: similar plot as that of fig. 4 for the candidate resonant peak at $E_x = 94.5$ MeV with the condition $\Delta_{RD} \leq 0.10$ for rod (upper panels) and tube (lower panels) shape. Right: χ^2 value distributions as a function of E_{th} (MeV).

resonant peak at $E_x = 94.5$ MeV. The global χ^2 value distributions are very similar in each other, indicating they are essentially governed by their outer shapes. However with a close look at the E_α distributions on the left column, one can easily recognize that the peak position of the simulation for the rod shape (upper panel) is about 5 MeV lower than that of the experiment. This situation is significantly improved in the case of the tube shape, even though the χ^2_{Ek} value changes only from 1.8 to 1.2. The average L_z values also shows significant differences in the two cases, because their moments of inertia required to get the same E_{rot} value are quite different. This tube shape preference over rod shape is observed for all candidate resonant peaks at $E_x \geq 86.5$ MeV.

9. – Summary

Twelve candidate resonant peaks for the high-spin resonant states, observed in the standard deviation with non-statistical nature from the excitation energy spectra of different decay channels, are investigated to characterize their shapes and angular momenta. Two of the lowest peaks do not show a shape preference. One at the highest energy (140 MeV) does not have enough statistics. For the other nine peaks their shapes and angular momenta are suggested as tube shapes with $L_z \geq 20\hbar$, indicating that they are possibly high-spin resonant states. The evaluated angular momentum values are consistent with those of the prediction made by Ren *et al.* in ref. [5] based on a mean-field calculation, but, within the constraints of the present analysis, their extracted shapes are tube shape, not toroidal. Given the strong correlation of the experimental excitation energies with the theoretical predictions [4, 5] for toroidal resonances, it is possible that this observation is a reflection of the de-excitation paths of the de-exciting resonant nuclei rather than their primary shapes. This possibility requires further investigation.

* * *

I thank A. Bonasera and L. Sobotka for useful discussions. This work is also supported by the US Department of Energy under Grant No. DE-FG02-93ER40773.

REFERENCES

[1] Wong C. Y., *Phys. Lett. B*, **41** (1972) 446.
[2] Wong C. Y., *Ann. Phys. (N.Y.)*, **77** (1973) 279.
[3] Wong C. Y., *Phys. Rev. C*, **17** (1978) 331.
[4] Staszczak A. and Wong C. Y., *Phys. Lett. B*, **738** (2014) 401.

[5] Ren Z. X. *et al.*, *Nucl. Phys. A*, **996** (2020) 121696.
[6] Cao X. G. *et al.*, *Phys. Rev. C*, **99** (2019) 014606.
[7] Hannaman A. *et al.*, *Phys. Rev. C*, **109** (2024) 054615.
[8] Gimeno-Nogues F. *et al.*, *Nucl. Instrum. Methods A*, **399** (1997) 94.
[9] Aslin M. *et al.*, *Nucl. Instrum. Methods A*, **985** (2021) 164674.
[10] Hannaman A. *et al.*, *Nucl. Instrum. Methods A*, **1050** (2023) 168130.
[11] Ono A. *et al.*, *Prog. Theor. Phys.*, **87** (1992) 1185.
[12] Ono A. *et al.*, *Phys. Rev. C*, **53** (1996) 2958.
[13] Ono A., *Phys. Rev.C*, **59** (1999) 853.
[14] Bondorf J. P. *et al.*, *Phys. Lett. B*, **240** (1990) 28 and references therein.
[15] Maruyama T. *et al.*, *Phys. Rev. C*, **53** (1996) 297.